Upgrading SuperKEKB with a Polarized Electron Beam: Discovery Potential and Proposed Implementation

PRE-DRAFT TEMPLATE October 2020

SuperKEKB e- Polarization Upgrade Working Group [1]

1 Introduction

A potential upgrade of the SuperKEKB e^+e^- collider with a polarized electron beam will open a new program of precision electroweak physics at the centre-of-mass energy of the $\Upsilon(4S)$ and is currently being considered. These measurements include $\sin^2\theta_W$ obtained via left-right asymmetry measurements of e^+e^- transitions to pairs of electrons, muons, taus, charm and b-quarks. The precision obtainable at SuperKEKB will match that of the LEP/SLC world average but at the centre-of-mass energy of 10.58 GeV, thereby probing the neutral current couplings with unprecedented precision at a new energy scale sensitive to the running of the couplings. World average measurements of the individual neutral current vector coupling constants to b- and c-quarks and muons in particular will be substantially improved and the residual 3σ discrepancy between the SLC A_{LR} and LEP A^b_{FB} measurements will be addressed. Precision measurements of neutral current universality will be more than an order of magnitude more precise than currently available, with measurements sensitive to parity-violating dark sector gauge bosons. Other physics enabled with polarized beams includes improved measurements of the properties of the tau lepton and searches for lepton flavour violation as well as topics in hadronic physics. This paper will include a discussion of the upgrades to SuperKEKB necessary to access this physics: polarized electron source, spin rotators, and Compton polarimetry. Polarimetry at the interaction point with tau lepton pairs will also be described. This program opens an exciting new window in searches for physics beyond the standard model.

The SuperKEKB e^+e^- collider operating at a centre-of-mass energy of 10.58 GeV, with its high design luminosity of 8×10^{35} cm^{-2} s^{-1}, can access new windows for discovery with the Belle II experiment if it is upgraded to have a longitudinally polarized electron beam. The target integrated luminosity for SuperKEKB/Belle II is 50 ab^{-1}[1] and currently Belle II is projected to collect that amount of data, which will not have beam polarization without an upgrade to SuperKEKB, by 2027. Upgrading SuperKEKB to have electron beams with left and right longitudinal polarization of approximately 70% at the Belle II interaction point creates a unique and versatile facility for probing new physics with precision electroweak measurements that no other experiments, current or planned, can achieve.

The upgrade to SuperKEKB involves three hardware projects:
1) A low-emittance polarized electron source in which the electron beams would be produced via a polarized laser illuminating a "strained lattice" GaAs photocathode as was done for SLD [2]. The source would produce longitudinally polarized electron bunches whose spin would be rotated to be transversely polarized before it enters the SuperKEKB electron storage ring;
2) A pair of spin-rotators, one positioned before and the other after the interaction region, to rotate the spin to longitudinal prior to collisions and back to transverse following collisions. One configuration under consideration for the spin-rotator is a combined function magnet that replaces an existing dipole in the SuperKEKB electron beam lattice with a superconducting magnet that has both a dipole and solenoid [6] as well as six skew quads. The challenge is to design the rotators to minimize couplings between vertical and horizontal planes and to address higher order and chromatic effects in the design to ensure the luminosity is not degraded;
3) A Compton polarimeter that measures the beam polarization before the beam enters the interaction region.

The rest of this paper provides more details of the physics discovery potential and the how electron polarization can be implemented in an upgrade to SuperKEKB while maintaining the high lumonisity.

2 Physics Case

A data sample of 20 ab^{-1} with a polarized electron beam enables Belle II to measure the weak neutral current vector coupling constants of the b-quark, c-quark and muon at significantly higher precision than any previous experiment. With 40 ab^{-1} of polarized beam data, the precision of the vector couplings to the tau and electron can be measured at a level comparable to current world averages, which are dominated by LEP and SLD measurements at the Z^0-pole.

Within the framework of the Standard Model (SM) these measurements of g_V^f, the neutral current vector coupling for fermion f, can be used to determine the weak mixing angle, θ_W, through the relation: $g_V^f = T_3^f - 2Q_f \sin^2\theta_W$,

[1] Names and institutions of SuperKEKB e- Polarization Upgrade Working Group Members

where T_3^f is the 3^{rd} component of weak isospin of fermion f, Q_f is its electric charge in units of electron charge and the notational conventions of Reference [2] are used.

As described in Reference [3], with polarized electron beams an e^+e^- collider at 10.58 GeV can determine g_V^f by measuring the left-right asymmetry, A_{LR}^f, for each identified final-state fermion-pair in the process $e^+e^- \to f\bar{f}$:

$$A_{LR}^f = \frac{\sigma_L - \sigma_R}{\sigma_L + \sigma_R} = \frac{sG_F}{\sqrt{2}\pi\alpha Q_f} g_A^e g_V^f \langle Pol \rangle \tag{1}$$

where $g_A^e = T_3^e = -\frac{1}{2}$ is the neutral current axial coupling of the electron, G_F is the Fermi coupling constant, s is the square of the centre-of-mass energy, and

$$\langle Pol \rangle = \frac{1}{2}\left[\left(\frac{N_{eR} - N_{eL}}{N_{eR} + N_{eL}}\right)_{\mathbf{R}} - \left(\frac{N_{eR} - N_{eL}}{N_{eR} + N_{eL}}\right)_{\mathbf{L}}\right] \tag{2}$$

is the average electron beam polarization, where N_{eR} is the number of right-handed electrons and N_{eL} the number of left-handed electrons in the event samples where the electron beam bunch is left polarized or right polarized, as indicated by the '**L**' and '**R**' subscripts. These asymmetries arise from $\gamma - Z$ interference and although the SM asymmetries are small (-6×10^{-4} for the leptons, -5×10^{-3} for charm and -2% for the b-quarks), unprecedented precisions can be achieved because of the combination of both the high luminosity of SuperKEKB and a 70% beam polarization measured with a precision of better than $\pm 0.5\%$. Note that higher order corrections are ignored here for simplicity, although studies at higher orders have recently begun [4].

The high precisions are possible at such an upgraded SuperKEKB because with 20 ab^{-1} of data Belle II can identify between 10^9 and 10^{10} final-state pairs of b-quarks, c-quarks, taus, muons and electrons with high purity and reasonable signal efficiency, and because all detector-related systematic errors can be made to cancel by flipping the laser polarization from **R** to **L** in a random, but known, pattern as collisions occur. $\langle Pol \rangle$ would be measured in two ways. The first method uses a Compton polarimeter, which can be expected to have an absolute uncertainty at the Belle II interaction point of less than 1% and provides a 'bunch-by-bunch' measurement of $\left(\frac{N_{eR}-N_{eL}}{N_{eR}+N_{eL}}\right)_{\mathbf{R}}$ and $\left(\frac{N_{eR}-N_{eL}}{N_{eR}+N_{eL}}\right)_{\mathbf{L}}$. The uncertainty will be dominated by the need to predict the polarizatoin loss from the Compton polarimeter to the interaction point. The second method measures the polar angle dependence of the polarization of τ-leptons produced in $e^+e^- \to \tau^+\tau^-$ events using the kinematic distributions of the decay products of the τ separately for the **R** and **L** data samples. The forward-backward asymmetry of the tau-pair polarization is linearly dependent on $\langle Pol \rangle$ and therefore can be used to determine $\langle Pol \rangle$ to 0.5% at the Belle II interaction point in a manner entirely independent of the Compton polarimeter. The τ polarization forward-backward asymmetry method avoids the uncertainties associated with tracking the polarization losses to the interaction point and also automatically accounts for any residual positron polarization that might be present. In addition, it automatically provides a luminosity-weighted beam polarization measurement.

Table 1 provides the sensitivities to electroweak parameters expected with polarized electron beams in an upgraded SuperKEKB from $e^+e^- \to b\bar{b}$, $e^+e^- \to c\bar{c}$, $e^+e^- \to \tau^+\tau^-$, $e^+e^- \to \mu^+\mu^-$, and $e^+e^- \to e^+e^-$ events selected by Belle II. From this information the precision on the b-quark, c-quark and muon neutral current vector couplings will improve by a factor of four, seven and five, respectively, over the current world average values[2] with 20 ab^{-1} of polarized data.

This is of particular importance for g_V^b, where the measurement of -0.3220$\pm$0.0077 is 2.8σ higher than the SM value of -0.3437 [2]. That discrepancy arises from the 3σ difference between the SLC A_{LR} measurements and LEP A_{FB}^b measurements of $\sin^2\theta_W^{eff}$. A measurement of g_V^b at an upgraded SuperKEKB that is four times more precise and which avoids the hadronization uncertainties that are a significant component of the uncertainties of the measurement of the forward-backward asymmetry at LEP, or any other forward-backward asymmetry measurement using on-shell Z^0 bosons, will be able to definitively resolve whether or not this is a statistical fluctuation or a first hint of a genuine breakdown of the SM.

Table 1 also indicates the uncertainties on $\sin^2\theta_W^{eff}$ that can be achieved with 40 ab^{-1} of polarized beam data - the combined uncertainty at Belle II would be comparable to the Z^0 world average measured uncertainty of ± 0.00016 from LEP and SLD[2] but made at a significanlty lower energy scale. Figure 1(left) shows the determinations of $\sin^2\theta_W$ as a function of energy scale at present and future experimental facilities including SuperKEKB upgraded with a polarized electron beam delivering 40 ab^{-1} of data to Belle II.

This electroweak program with polarized electron beams in SuperKEKB would provide the highest precision tests of neutral current vector coupling universality. In addition, right-handed b-quark couplings to the Z can be experimentally probed with high precision at Belle II with polarized beams. Also, measurements with the projected precision will enable Belle II to probe parity violation induced by the exchange of heavy particles such as a hypothetical TeV-scale Z' boson(s). If such bosons only couple to leptons they will not be produced at the

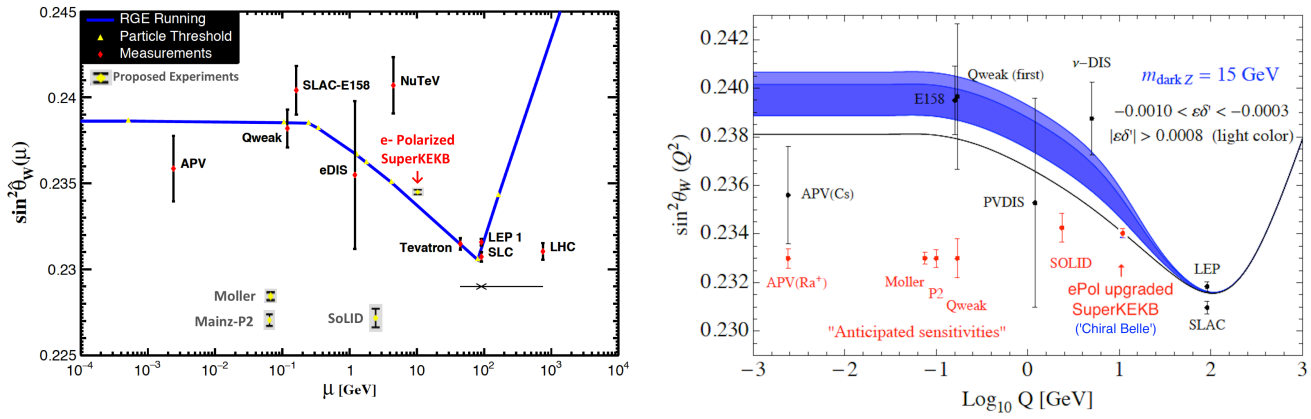

Figure 1: Left: Determination of $\sin^2\theta_W$ at present and future experimental facilities as a function of energy scale, adapted from [5]. Right: Dark blue band shows Q^2-dependent shift in $\sin^2\theta_W$ caused by a 15 GeV mass dark Z, adapted from [11].

LHC. Moreover, the SuperKEKB machine will have a unique possibility to probe parity violation in the lepton sector mediated by light and very weakly coupled particles often referred to as "Dark Forces". Such forces have been entertained as a possible connecting link between normal and dark matter [7, 8]. SuperKEKB with polarization would be uniquely sensitivity to "Dark Sector" parity violating light neutral gauge bosons,especially when Z_{dark} is off-shell and with a mass between roughly 10 and 35 GeV [11] or even up to the Z^0 pole, or couples more to the 3rd generation (see Figure 1(right)).

The enhancement of parity violation in the muon sector has been an automatic consequence of some models [9] that aim at explaining the unexpected result for the recent Lamb shift measurement in muonic hydrogen [10]. The left-right asymmetry of the $e^-e^+ \to \mu^-\mu^+$ in such models is expected to be enhanced at low-to-intermediate energies, and SuperKEKB with polarized beams may provide a conclusive test of such models, as well as impose new constraints on a parity-violating dark sector.

Final State Fermion	A_{LR}^{SM}	Relative A_{LR} Error (%)	g_V^f W.A.[2]	$\sigma(g_V^f)$ (20 ab^{-1})	$\sigma(g_V^f)$ (40 ab^{-1})	$\sigma(s^2\theta_W)$ (40 ab^{-1})
b-quark (eff.=0.3)	-0.020	0.5	-0.3220 $\pm$0.0077	0.002 improves x4	0.002	0.003
c-quark (eff.=0.3)	-0.005	0.5	+0.1873 $\pm$0.0070	0.001 improves x7	0.001	0.0007
tau (eff.=0.25)	-0.0006	2.3	-0.0366 $\pm$0.0010	0.0008	0.0006	0.0003
muon (eff.=0.5)	-0.0006	1.5	-0.03667 $\pm$0.0023	0.0005 improves x5	0.0004	0.0002
electron (1 nb acceptance)	-0.0006	1.2	-0.3816 $\pm$0.00047	0.0004	0.0003	0.0002

Table 1: For each fermion pair cleanly identifiable in Belle II for the given efficiency in column 1: column 2 gives the SM value of A_{LR}; column 3, the expected relative error on A_{LR} based on based on 20 ab^{-1} and a beam polarization at Belle II of 70% with an error of $\pm$0.5%; column 4, the current world average value of its neutral current vector coupling; column 5, the projected error on g_V^f with 20 ab^{-1} of data; column 6, the projected error on g_V^f with 40 ab^{-1} of data; and column 7, the projected SuperKEKB/Belle II error on $\sin^2\theta_W^{eff}$ with 40 ab^{-1} of polarized e$^-$ beam data.

3 Polarized Source

4 Spin Rotator

4.1 BINP Spin Rotator Conceptual Design

HER storage ring transformations to obtain longitudinal polarization of electrons at the SuperKEKB interaction point

I.A.Koop, A.V. Otboev, Yu.M. Shatunov, BINP SB RAS, 630090 Novosibirsk

Introduction

This paper discusses the problems of obtaining longitudinal polarization in future experiments of the BELLE-2 collaboration at the SuperKEKB electron-positron collider [1].

Due to the extremely small coupling coefficient of transverse oscillations in SuperKEKB [2, 3]: $\varepsilon_y/\varepsilon_x \approx 0.002$, it seems absolutely impossible to use any spin rotator schemes using transverse dipole fields. Only the scheme with the use of a longitudinal magnetic field has no effect on the value of the vertical emittance, which is formed by quantum fluctuations of synchrotron radiation in the main dipole magnets of the ring and by parasitic coupling of transverse oscillations.

The concept of a scheme for obtaining longitudinal polarization

Below, we discuss the simplest version of such a scheme of rotations of the direction of the electron spin vector, when the vertical direction of the spin in the main arcs is completely restored when the beam passes through a long experimental straight section of the HER ring [4, 5], see Fig. 1.

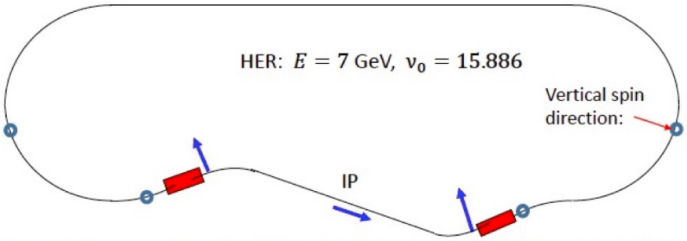

Spin direction is vertical in the main part of HER. Then it is rotated to the horizontal plane by the set of two solenoids, which are comprising the 90^0 spin rotator.

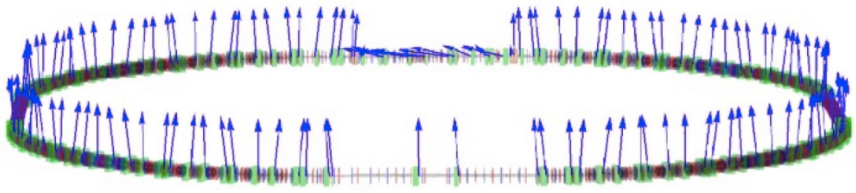

Fig. 1 Scheme of spin rotations with restoration of their vertical direction in the main arcs of the ring. Each spin rotator consists of two solenoids and several skew-quadrupole lenses that compensate for the coupling of betatron oscillations introduced by these solenoids.

The left and right spin rotators have the opposite sign of the longitudinal magnetic field, and the whole rotation scheme is generally antisymmetric in the signs of magnetic fields at an equilibrium orbit. This antisymmetry ensures almost complete absence of the dependence of the spin orientation in the loops on the particle energy, which is very important for obtaining a long beam depolarization time. The presence of a nonzero dispersion function in spin rotators and magnets between them does not allow to completely suppress the chromatic energy dependence of the spin orbit in the loops. We will discuss this issue in greater details later.

To rotate the electron spin by 90 degrees, the field integral in the solenoids is proportional to the particle momentum:

$$Bl = \frac{\pi}{2(1+a_e)}BR$$

Here $BR = pc/e$ - magnetic rigidity, $a_e \approx 1.16 \cdot 10^{-3}$ – anomalous magnetic moment of an electron.

The subsequent rotation of the spin by 90^0 in the horizontal plane occurs in the section from the rotator to the point of intersection of the beams with the total angle of rotation of the velocity vector equal to:

$$\theta = \frac{\pi}{2\nu_0}$$

where $\nu_0 = \gamma a_e$ is the dimensionless spin frequency (or tune) proportional to the gamma factor of the particle.

To detune from resonances with betatron oscillation frequencies, which can quickly depolarize the beam due to beam-beam collision effects, we chose the optimal value of the electron energy equal to $E = 7.15$ GeV, which corresponds to the spin tune $\nu_0 = 16.226$ – sufficiently distant both from close to half-integer values of transverse oscillation frequencies, and from integer resonances with their synchrotron satellites. This value of the spin tune dictates to us the required total angle of all turns in the horizontal plane from the rotator to the interaction point equal to $\theta = 0.0968$.

In the current geometry of the complicated wavy HER orbit, there is no suitable place for a spin rotator. Moreover, given that the length of the rotator is about 10 meters, several dipoles had to be moved from their places, simultaneously changing their angles of rotation. Such transformations of the long insertion connecting the left and right arches were calculated and optimized taking into account the preservation of the storage ring perimeter. The geometries of the separation of the trajectories of the LER and HER rings are slightly different on the left and right sides from the interaction point, see respectively Fig. 2 and Fig. 3.

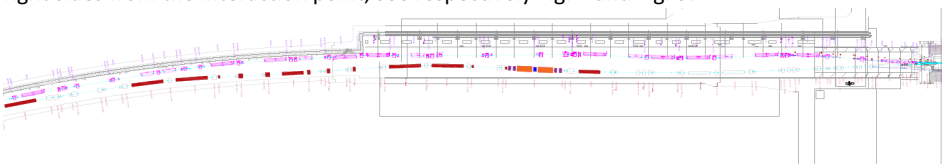

Fig. 2 To the left from the IP half of experimental straight section. The modified magnetic elements of the HER ring are painted in dark brown, and the solenoids of the spin rotator are painted in dark yellow. The distance between the rings is great enough everywhere.

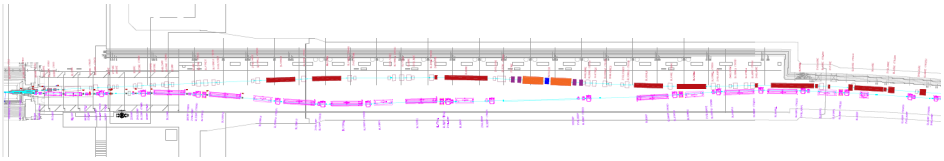

Fig. 3 To the right from the IP half of straight section. At the entrance to the tunnel, the magnets of the rings are very close, but all technical problems can obviously be solved.

In a condensed form, the scheme of intersection of the collider rings is shown in Fig. 4.

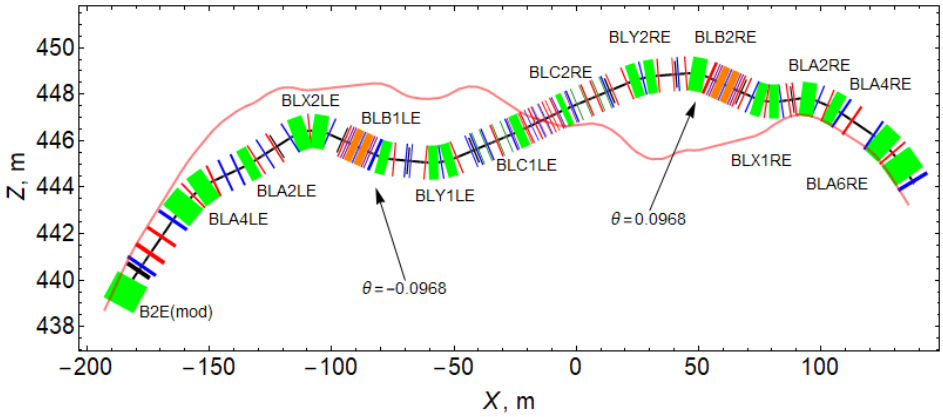

"B2E(mod)"	"BLA2LE"	"BLA2RE"	"BLA4LE"	"BLA4RE"	"BLA6RE"	"BLB1LE"
0.0745895	−0.0181419	0.0591537	0.0520765	0.0280687	0.0501498	−0.0368136

"BLB2RE"	"BLC1LE"	"BLC2RE"	"BLX1RE"	"BLX2LE"	"BLY1LE"	"BLY2RE"
0.0548871	−0.00591049	0.0059199	−0.0310501	0.0570931	−0.0270415	0.018

Fig.4 Optimized SuperKEKB ring intersection scheme for longitudinal polarization. Spin rotators are located in convenient places, away from the tunnel walls and the magnetic elements of the positron ring. The angles of rotation of all dipole magnets are given at the bottom of the diagram, and in Tables 1 and 2. The lengths and angles of only modified dipoles are given.

Table 1. Lengths and rotation angles of the dipoles to the left of the intersection of the beams.

		Original parameters of dipoles		New parameters	
Name	Quantity	Length, m	Angle, rad	Length, m	Angle, rad
B2E.4	1	5.90220	0.0557427	5.90220	0.0745895
BLA4LE	2	5.90220	0.0663658	5.90220	0.0520765
BLA2LE	1	5.90220	0.0206421	3.96143	- 0.0181419
BLX2LE	2	3.96143	0.0259281	5.90220	0.0570931
BLB1LE	1	3.96143	-0.0229996	3.96143	-0.0368136

Table 2. Lengths and rotation angles of the dipoles to the right of the intersection of the beams.

		Original parameters of dipoles		New parameters	
Name	Quantity	Length, m	Angle, rad	Length, m	Angle, rad
BLA6RE	2	5.90220	0.0501497	5.90220	0.0501498
BLA4RE	1	5.90220	0.0480687	3.96143	0.0280687
BLA2RE	1	3.96143	0.0348280	5.90220	0.0591537
BLX1RE	2	3.96143	-0.0221788	3.96143	-0.0310501
BLB2RE	1	3.96143	0.0234696	5.90220	0.0548871
BLY2RE	2	3.96143	0.0270000	3.96143	0.0180000

HER storage ring transformations to obtain longitudinal polarization of electrons at the SuperKEKB interaction point

I.A.Koop, A.V. Otboev, Yu.M. Shatunov, BINP SB RAS, 630090 Novosibirsk

Introduction

This paper discusses the problems of obtaining longitudinal polarization in future experiments of the BELLE-2 collaboration at the SuperKEKB electron-positron collider [1].

Due to the extremely small coupling coefficient of transverse oscillations in SuperKEKB [2, 3]: $\varepsilon_y/\varepsilon_x \approx 0.002$, it seems absolutely impossible to use any spin rotator schemes using transverse dipole fields. Only the scheme with the use of a longitudinal magnetic field has no effect on the value of the vertical emittance, which is formed by quantum fluctuations of synchrotron radiation in the main dipole magnets of the ring and by parasitic coupling of transverse oscillations.

The concept of a scheme for obtaining longitudinal polarization

Below, we discuss the simplest version of such a scheme of rotations of the direction of the electron spin vector, when the vertical direction of the spin in the main arcs is completely restored when the beam passes through a long experimental straight section of the HER ring [4, 5], see Fig. 1.

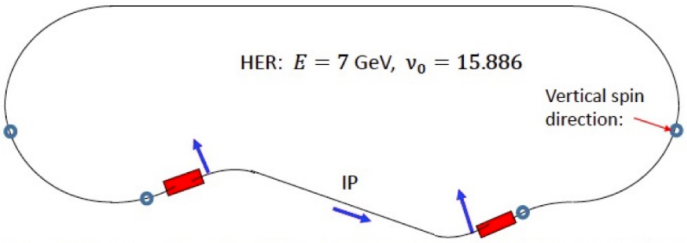

Spin direction is vertical in the main part of HER. Then it is rotated to the horizontal plane by the set of two solenoids, which are comprising the 90^0 spin rotator.

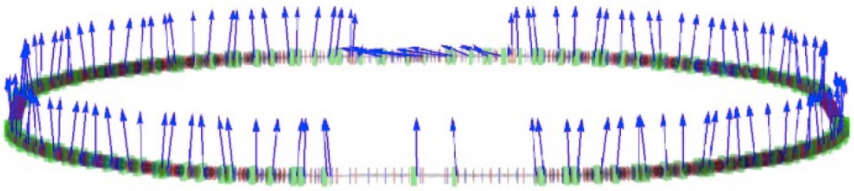

Fig. 1 Scheme of spin rotations with restoration of their vertical direction in the main arcs of the ring. Each spin rotator consists of two solenoids and several skew-quadrupole lenses that compensate for the coupling of betatron oscillations introduced by these solenoids.

The left and right spin rotators have the opposite sign of the longitudinal magnetic field, and the whole rotation scheme is generally antisymmetric in the signs of magnetic fields at an equilibrium orbit. This antisymmetry ensures almost complete absence of the dependence of the spin orientation in the loops on the particle energy, which is very important for obtaining a long beam depolarization time. The presence of a nonzero dispersion function in spin rotators and magnets between them does not allow to completely suppress the chromatic energy dependence of the spin orbit in the loops. We will discuss this issue in greater details later.

s on the AmPS storage ring at NIKHEF, Amsterdam [7].

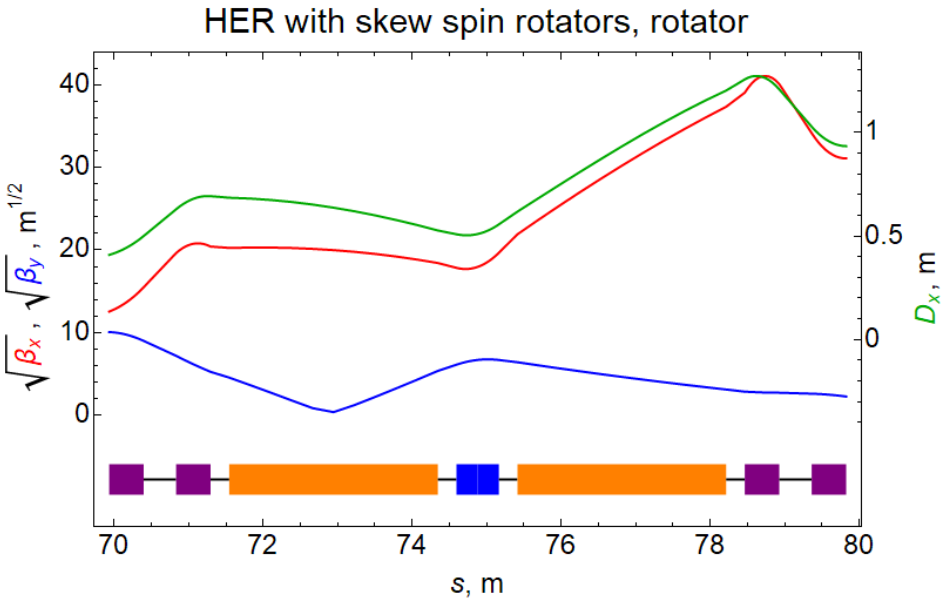

Fig. 5 Optical functions of the spin rotator for the left half of the long interaction region.

The middle lens is not rotated around its axis, while the lenses of the two outermost doublets are rotated at an angle $\varphi = \pm\pi/8(1 + a_e) = \pm\, 22.474^0$.

The *X*-box 2x2 matrix is:

$$T = \begin{pmatrix} 0.4134 & 7.13 \\ -0.14025 & 0.4134 \end{pmatrix}$$

The total length of the rotator is 9.89112 meters. Table 3 shows the main parameters of the solenoids and lenses of this spin rotator.

Table 3. Basic parameters of lenses and solenoids for *BR* = 23.3495 T·m (*E* = 7.15 GeV).

Element	Length, m	Field or Gradient: T, T/m
Quadrupole #1, #5	0.46227	-29.4792 ($\varphi 1 = -\varphi 5 = -22.474^0$)
Drift 1	0.436	
Quadrupole #2, #4	0.46227	28.5569 ($\varphi 2 = -\varphi 4 = -22.474^0$)
Drift 2	0.25	
Solenoid	2.8	6.54197
Drift 3	0.25	
Quadrupole #3	0.57004	-25.3736 ($\varphi 3 = 0$)

Alternatively, we consider the option of combining the solenoidal and quadrupole fields. This approach has already been discussed in [5], but with a more radical proposal - to combine three types of fields: solenoidal, quadrupole, and dipole. But, as we have already said, the presence

of a dipole field leads to the excitation of too large vertical emittance. Table 4 shows the parameters of quadrupole lenses of such a combined version, in which the solenoidal field is continuous and occupies the entire length of the rotator of 9.2 m.

The windings of the quadrupole lenses are superimposed on a cylindrical mandrel over the solenoid winding. Moreover, there are two sets of windings: straight-oriented windings and weaker second windings rotated at an angle of 45^0 to them, creating a skew-quadrupole field. The total number of lenses in the rotator is increased to 7 in order to have the freedom to reproduce the same optics in the versions with the longitudinal field on and off.

Table 4. Basic parameters of lenses and solenoids of a spin rotator with a superposition of solenoidal and quadrupole fields for *BR* = 23.3495 T·m (*E* = 7.15 GeV). The sequence of numbering of structure elements: 1, 2,…, 17.

Element	Length, m	Field or Gradient: T, T/m
Drift #1, #17	0.34556	$B_s = G = 0$
Pure Solenoid #2, #16	0.15	$B_s = 4.067373$
Quadrupole plus Solenoid: #3, #15	0.7	-20.067768 ($\varphi 3 = -\varphi 15 = -19.822^0$)
Solenoid #4, #14	0.4	$B_s = 4.067373$
Quadrupole plus Solenoid: #5, #13	0.7	23.232294 ($\varphi 5 = -\varphi 13 = -14.5297^0$)
Solenoid #6, #12	0.8	$B_s = 4.067373$
Quadrupole plus Solenoid: #7, #11	0.7	-5.385630 ($\varphi 7 = -\varphi 11 = -7.3598^0$)
Solenoid #8, 10	0.8	
Quadrupole plus Solenoid: #9	0.7	-22.806964 ($\varphi 9 = 0$)

The option with combined fields has several attractive points. Its main advantage over the variant with separated functions is the small value of the longitudinal field: $B_s = 4.067373$ T versus alternative $B_s = 6.54197$ T. Also, the use of a common cylindrical frame supporting both the solenoidal and quadrupole windings may be more technologically advanced as compared to their separate fixation in space. In addition, the need to create two types of lens windings - straight-oriented and skew-rotated - makes the cosine-theta technology the preferred choice.

When calculating the transport matrix of a section of the structure with superposition of the quadrupole and solenoidal fields constant along s, we used numerical methods for calculating the exponent of the matrix of a linear system of equations of motion:

$$\frac{dX}{ds} = A \cdot X \qquad A = \begin{pmatrix} 0 & 1 & \kappa & 0 \\ -\kappa^2 - g & 0 & 0 & \kappa \\ -\kappa & 0 & 0 & 1 \\ 0 & -\kappa & -\kappa^2 + g & 0 \end{pmatrix}$$

Transformation transport matrix of vector $X = (x, p_x, y, p_y)^T$ is equal:

$$T(s, g, \kappa) = R(-s\kappa)\exp(sA)R(s\kappa)$$

where $R(s\kappa)$ – the rotation matrix, and the arguments of the matrix A are as defined above. Note that p_x and p_y are canonical momenta, defined as:

$$p_x = x' - \kappa y$$
$$p_y = y' + \kappa x$$

Canonical momenta do not experience any jumps at the boundaries of the solenoidal field, in contrast to kinetic impulses x', y', which subjected a discontinuity at solenoid edges.

The angles of rotation of the lenses were selected in such a way as to make all elements of antidiagonal 2x2 coupling boxes of the complete transport matrix of the rotator vanish. To fulfill this condition, taking into account the mirror symmetry of the placement of all seven lenses and with the antisymmetric rotation of six of them around the axis, we used a procedure for numerical optimization of three rotation angles and gradients of four lens families (the central lens is not rotated!). The *X*-block matrix was selected the same as in the rotator version with separated longitudinal and transverse fields:

$$T = \begin{pmatrix} 0.4134 & 7.13 \\ -0.14025 & 0.4134 \end{pmatrix}$$

The matrix of the *Y*-block is equal to it with the opposite sign.

At the edges of the rotator, short drift gaps with a length of 0.34556 m are left free from fields, connecting the cold superconducting magnetic system with room temperature of the adjacent areas. The total length of the entire rotator is 9.89112 m, same as in the first version.

Beam depolarization time.

When a photon of synchrotron radiation is emitted, there is an abrupt change in the equilibrium direction of the spin and the magnitude of the projection of the spin on the new equilibrium direction. The spin relaxation time of the beam due to this process and the equilibrium degree of polarization are determined by the well-known Derbenev-Kondratenko formulas [10]:

$$\tau_{rad}^{-1} = \frac{5\sqrt{3}}{8}\lambda_e r_e c\gamma^5 \langle |r|^{-3} \left(1 - \frac{2}{9}(\vec{n}\vec{v})^2 + \frac{11}{18}\left(\vec{d}\right)^2\right)\rangle$$

$$\xi_{rad} = -\frac{8}{5\sqrt{3}} \frac{\langle |r|^{-3}\vec{b}(\vec{n} - \vec{d})\rangle}{\langle |r|^{-3} \left(1 - \frac{2}{9}(\vec{n}\vec{v})^2 + \frac{11}{18}\left(\vec{d}\right)^2\right)\rangle}$$

where $\lambda_e, r_e,\ c$ and γ – Compton wavelength of an electron, its classical radius, speed of light and gamma factor, respectively. Other parameters stands for: r – radius of curvature of the orbit at the point of emission of the photon, $\vec{b}$ – unit vector indicating the direction of the magnetic field, $\vec{n}$ - unit vector along the equilibrium spin direction at a given azimuth, $\vec{d} = \gamma(d\vec{n}/d\gamma)$ – spin-orbit coupling vector, showing the direction of the jump of vector $\vec{n}$ when a photon is emitted, and the magnitude of this jump.

Modulus distribution of vector $\vec{d}$ over the azimuth of the storage ring was calculated by the ASPIRRIN program, created in the 90s [8, 9]. Figure 6 shows the graph $\left|\vec{d}(s)\right|$ calculated for the

rotator optics option with the parameters in Table 3.

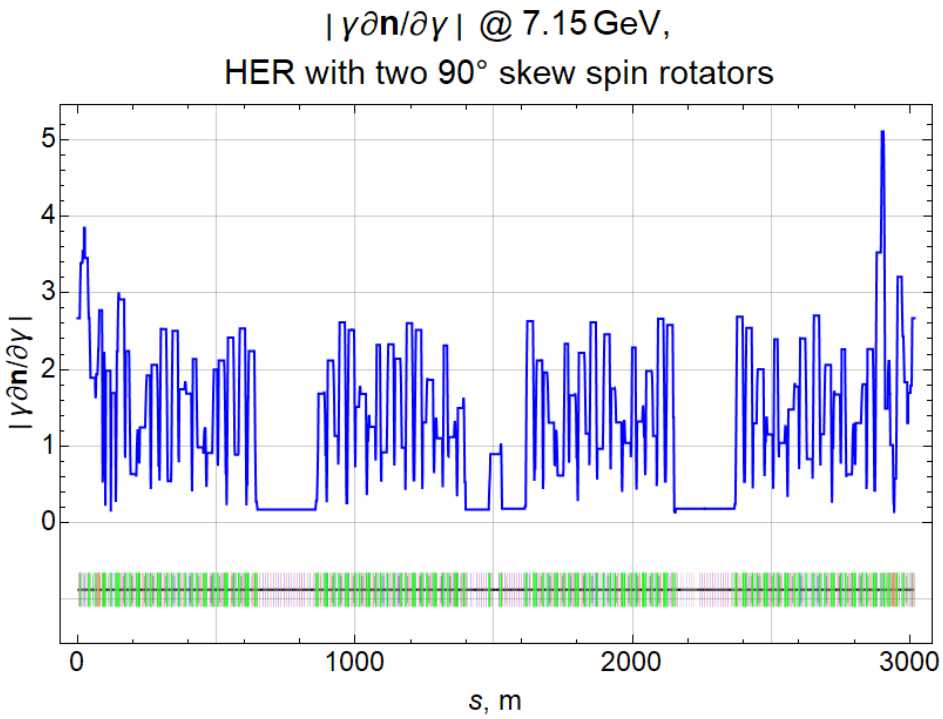

Fig.6 Graph of the modulus of the spin-orbit coupling vector in the HER ring with a modified rotation geometry in the experimental section. Rotator parameters from Table 3 and Fig. 5.

It is essential that for a given optimized value of the beam energy *E* = 7.15 GeV the modulus $|\vec{d}(s)|$ almost everywhere does not exceed the factor 2. Thereby the spin relaxation time falls from the initial values of the Sokolov-Ternov polarization time $\tau_{ST} = 32000$ s only to quite acceptable $\tau_{rad} = 10000$ s. This time remains very long in comparison with the time for refreshing the beam with new polarized electrons, which is less than $\tau_{beam} < 1000$ sec. The energy dependence of the radiation spin relaxation time is shown in Fig. 7. Resonances with integer values of the spin frequency occurred at the energy *E* = 6.61, 7.05, 7.49 GeV, and the so-called “intrinsic” spin resonances with the betatron vibration frequencies are located at the spin tunes $\{\nu_0\}$ =0.4 and 0.6. You have to choose the beam energy and operate somewhere in between these two types of resonances, for example at *E*=7.15 GeV, or in other words at spin tune $\nu_0 = 16.226$.

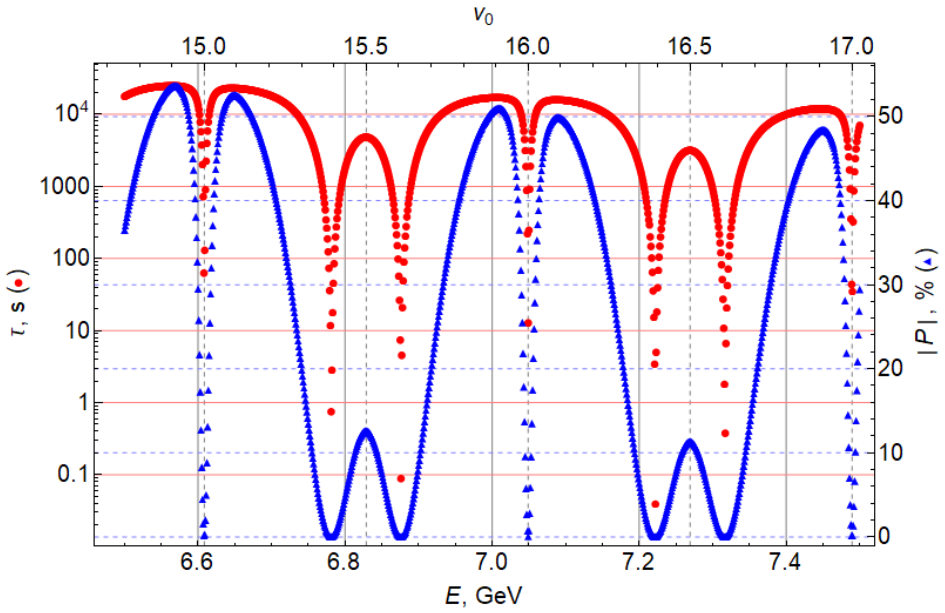

Fig.7 Dependence of the radiation spin relaxation time on energy with the rotator version from Table 3 with rotated extreme doublets of the lenses, see Fig. 5.

In principle, resonances with betatron frequencies can be made narrower. For this, it is necessary to fulfill the condition of the spin transparency of both: the rotator itself and the entire experimental straight section as a whole - from the rotator to the rotator [11]. But, as our study has shown, the fulfillment of the conditions for spin transparency requires several times stronger lenses in comparison with the variants of rotator optics considered above. Therefore, we have come to a compromise variant of using relatively weak lenses providing, nevertheless, a sufficiently long spin relaxation time. Note that electrons with the opposite sign of polarization with respect to the equilibrium one dictated by the Sokolov-Ternov self-polarization mechanism will depolarize much faster, tending exponentially to their natural state with a positive degree of polarization shown by the blue curve in Fig. 7. Apparently, bunches of electrons with a negative sign of polarization need to be updated more often so that their degree of polarization averaged over time is as high as for its positive sign.

Unfortunately, all programs of accelerator optics calculations available to us, such as MADx or RING, as well as the program for calculating the spin response functions ASPIRRIN, do not support the calculation of matrices of optical elements with combined longitudinal and quadrupole fields. Therefore, to calculate the time and degree of self-polarization in the variant of optics with combined longitudinal and quadrupole fields, we replaced the structure of rotators with a continuous longitudinal field (Table 4) with a structure similar to it presented in Table 5. In this structure, longitudinal field discontinuities are made, in which somewhat shortened lenses are located at the same distances from each other between their centers, as in the variant of Table 4, see Fig. 8. The presence of four families of quadrupole lenses and complete freedom in choosing the angles of their rotation around the axis make it possible to obtain any betatron phase advances and periodic beta functions of the rotator, both with the

longitudinal field turned on and off. We reproduced the X-box matrix the same as the rotator shown in Fig. 5.

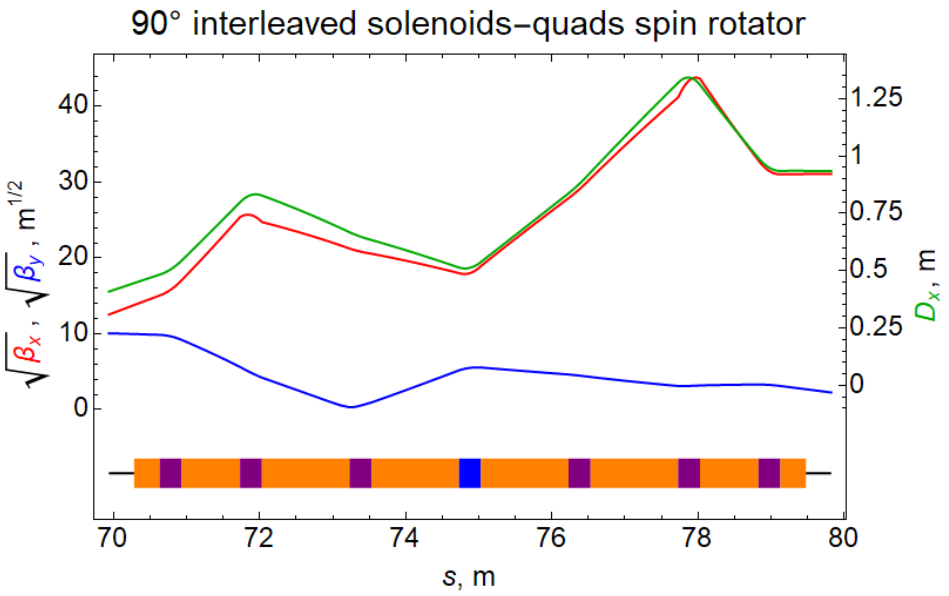

Fig.8 Amplitude functions in a rotator with alternating sections of solenoids and quadrupole lenses rotated around the axis.

Table 5. Parameters of lenses and solenoids of a spin rotator with alternating solenoidal and quadrupole fields for BR = 23.3495 T·m (E = 7.15 GeV).

Element and its sequence number	Length, m	Field or Gradient: T, T/m
Drift #1, #17	0.34556	$B_s = G = 0$
Solenoid #2, #16	0.35	$B_s = 5.15983$
Quadrupole: #3, #15	0.3	-41.5055 $(\varphi 3 = -\varphi 15 = -20.25818^0)$
Solenoid #4, #14	0.8	$B_s = 5.15983$
Quadrupole : #5, #13	0.3	45.5005 $(\varphi 5 = -\varphi 13 = -15.19364^0)$
Solenoid #6, #12	1.2	$B_s = 5.15983$
Quadrupole : #7, #11	0.3	-7.56501 $(\varphi 7 = -\varphi 11 = -7.59682^0)$
Solenoid #8, 10	1.2	$B_s = 5.15983$
Quadrupole : #9	0.3	-53.2734 $(\varphi 9 = 0)$

The magnitude of the modulus of the spin-orbit coupling vector calculated by the ASPIRRIN program is shown in Fig. 9. Its average value in the main part of the ring is less than one and it can be seen that this version of the rotator optics is the best of all those presented earlier. This was reflected in a significant increase in the spin relaxation time: $\tau_{rad} = 18800$ s versus 10000 s for the rotator version from Table 3. Both these tau-values are given for beam energy E = 7.15 GeV. The degree of equilibrium polarization also increased from P = 40% to P = 60%. The graphs of the dependence of the relaxation time and the equilibrium degree of polarization on energy

are shown in Fig. 10. We believe that the above estimates of radiative self-polarization refer not only to the version from Table 5, but also to the version of the parameters taken from Table 4 with a continuous longitudinal field.

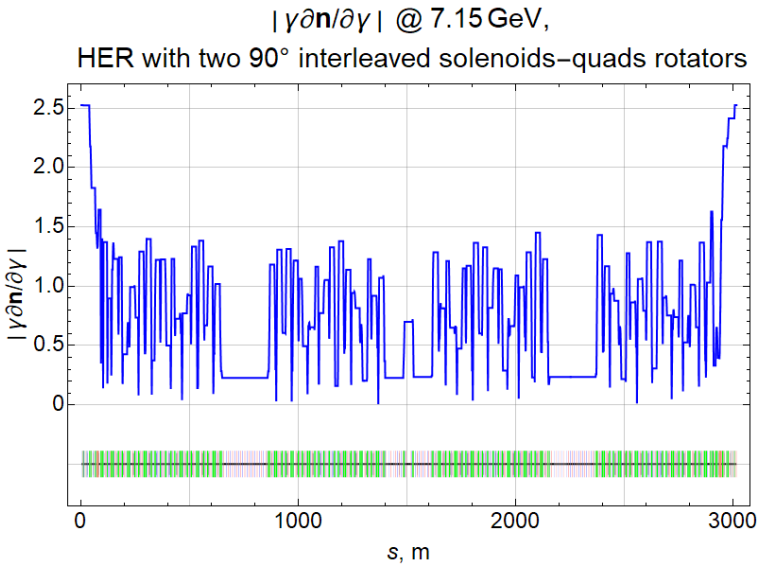

Fig.9 Modulus of the spin-orbit coupling vector in the HER ring with the rotator parameters from Table 5.

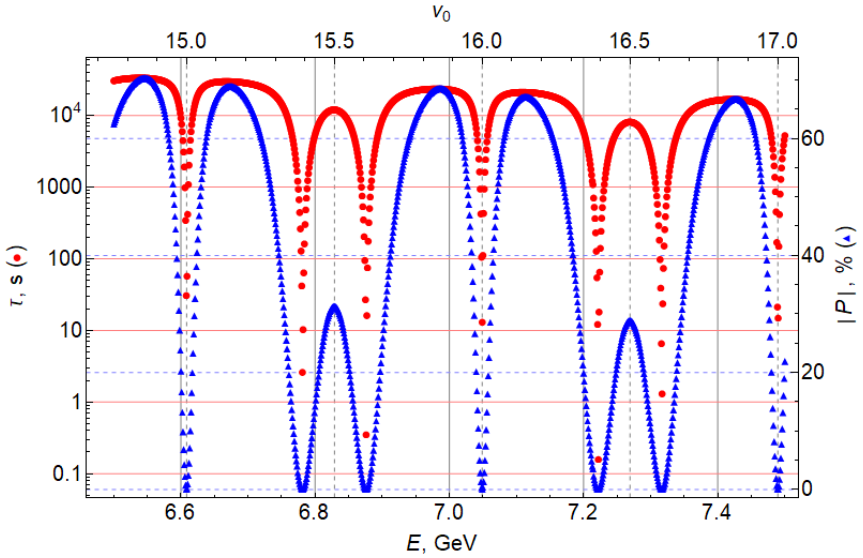

Fig 10. Radiation spin relaxation time and equilibrium degree of polarization versus energy for the rotator optics option from Table 5.

Finally, Figures 11-12 show the optical functions of the left and right halves of the long experimental straight section. They show spin rotators with an optical structure from Table 3. Outside the rotators, the beta functions and the dispersion function are the same for all the versions considered above, since the transport matrices of all these versions are made the same.

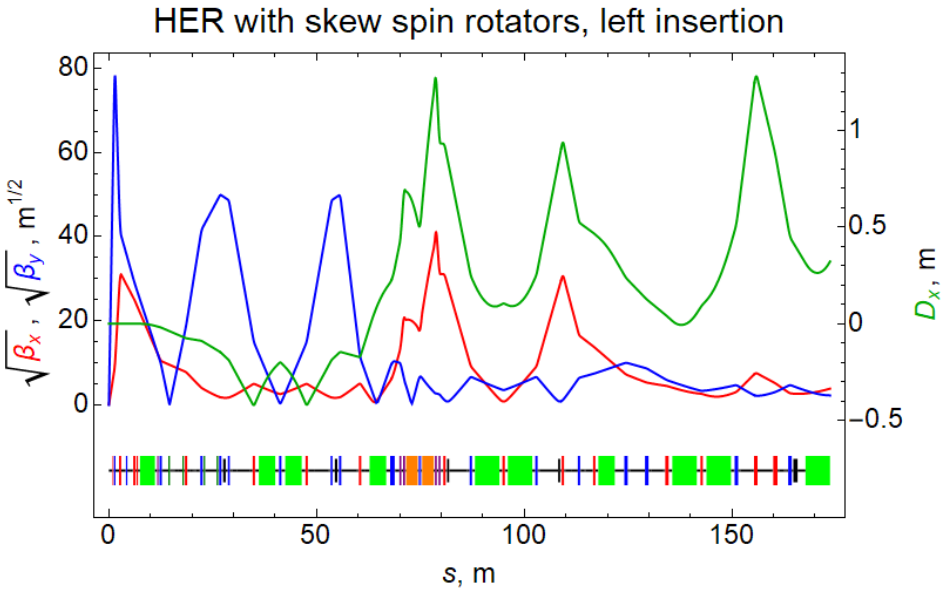

Fig. 11 Optical functions of the left half of the long experimental section.

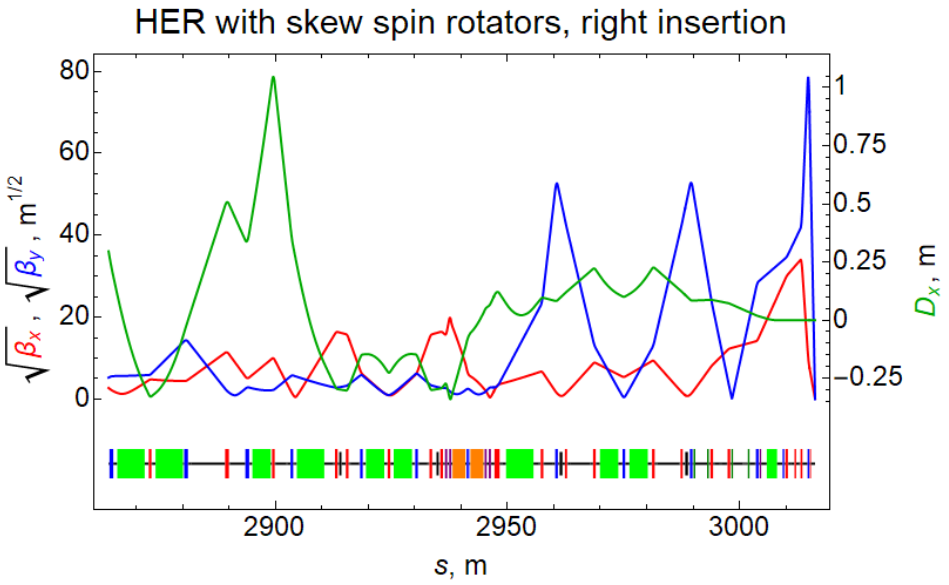

Fig. 12 Optical functions of the right half of the long experimental section.

Conclusion.

We found, in our opinion, an acceptable variant of converting the geometry of electron beam bends in the experimental section of the HER storage ring, which provides drift gaps with a length of about 10 meters for installing spin rotators in them. Two rotators serve to rotate electron spins by 90^0 from vertical to horizontal and then, after passing the crossing point, back to vertical.

Various lattice options for spin rotators are considered. In the variant with separate longitudinal and quadrupole transverse fields, the optimal transport matrix of the rotator was found, which made it possible to minimize the disturbances in the optics of the storage ring by the changes introduced. The disadvantage of this option is the relatively large value of the longitudinal magnetic field: over 6.54 T. This disadvantage is eliminated in the variant with the superposition of the rotated quadrupole fields on the continuous longitudinal field of the solenoid, which now occupies the entire length of the gap allocated for the rotator. The value of the longitudinal field in this variant dropped to 4.067 T.

Calculations of the relaxation time of polarization from the initial + 90% or -90% to its equilibrium value near + 60% showed its sufficiently large value, about 19000 sec, which will make it possible to have a very high level of average polarization during the lifetime of the beam with continuous feeding with new polarized electrons from injector.

The urgent task at the next stage is to check the boundaries of the dynamic aperture by tracking the particles in order to get an answer to the question of whether it has worsened in comparison with the initial version of the ring optics.

References.

[1] M. Roney, “Polarized Electron Beams in a SuperKEKB Upgrade”, e- Polarization Session

B2GM 34, KEK, 23 August 2019.

[2] Y. Ohnishi, H. Koiso, A. Morita, H. Sugimoto, and K. Oide, “LATTICE DESIGN OF LOW EMITTANCE AND LOW BETA FUNCTION AT COLLISION POINT FOR SuperKEKB”, Proceedings of IPAC2011, San Sebastián, Spain THPZ007.

[3] Y. Onishi on behalf of the SuperKEKB accelerator group, “Start of SuperKEKB”, 38th International Conference on High Energy Physics 3-10 August 2016 Chicago, USA. Published in PoS ICHEP2016 (2016) 006, pp.8.

[4] I. Koop, A. Otboev and Yu. Shatunov, “Issues and Challenges for Longitudinal Polarization in SuperKEKB”, a talk given at BELLE-II Collaboration Meeting. February 2020, Tsukuba.

[5] U. Wienands, ANL-APS and N. Wang, U. of Illinois Urbana-Champaign (Lee Teng Student), “A Compact Spin Rotator”, 24-Jun-2020, Belle 2 GM.

[6] A.A. Zholents, V.N. Litvinenko, Preprint YAF 81-80 (1981), also in DESY-L-TRANS-289.

[7] G. Luijckx et al, “Polarized electrons in the AmPS storage ring”, Proc. of PAC1997, Vancouver, Canada, 1997, pp.1063-1065.

[8] V.I. Ptitsyn, PhD thesis, Novosibirsk, 1997, in Russian.

[9] V.I. Ptitsyn, Yu.M. Shatunov, S.R. Mane," Spin response formalism in circular accelerators", Nuclear Instruments and Methods in Physics Research A 608 (2009) 225–233.

[10] Ya.S.Derbenev, A.M.Kondratenko, "Polarization kinematics of particles in storage rings", Sov.Phys.JETP 37:968-973, 1973, Zh.Eksp.Teor.Fiz.64:1918-1929, 1973.

[11] I. A. Koop, A. V. Otboyev, P. Yu. Shatunov, and Yu. M. Shatunov, "Spin transparent Siberian Snake and Spin Rotator with solenoids", SPIN-2006, Kyoto, AIP Conference Proceedings 915, 948 (2007).

4.2 Combined Function Spin Rotator Conceptual Design

5 Compton Polarimetry

6 Tau Polarimetry

Due to the left handed nature of the weak nuclear force the τ particle is uniquely suited for gaining access to beam polarization. This is due in part to the τ decaying while inside the detector and secondly the kinematics of the decay products are sensitive to the τ chiral state. The τ spin state is coupled to the spin state of the beam that produced it and so the final decay products are also sensitive to the beam polarization. Figure 2 shows how the momenta of final state products are influenced beam polarization. As the $\tau \to \pi\nu$ decay is the most sensitive we will focus on a measurement using this decay mode. In the future this work could be extended to include the other decay modes for additional statistics. Table 2 shows the relevant tau decay branching fractions.

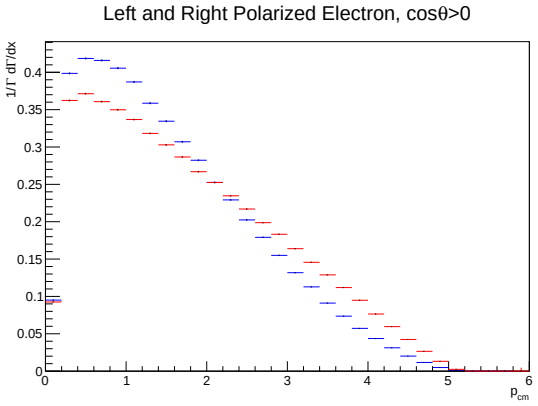

(a) $\tau \to e\nu\bar{\nu}$ momentum of final state particle

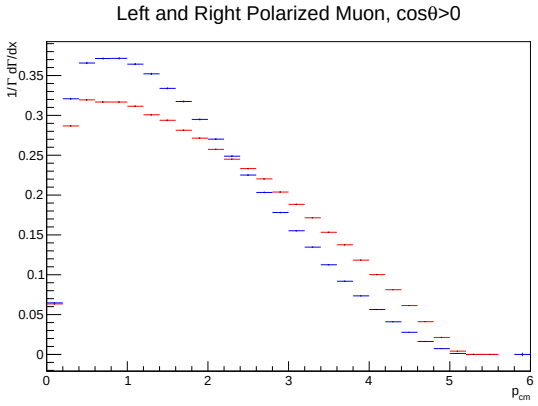

(b) $\tau \to \mu\nu\bar{\nu}$ momentum of final state particle

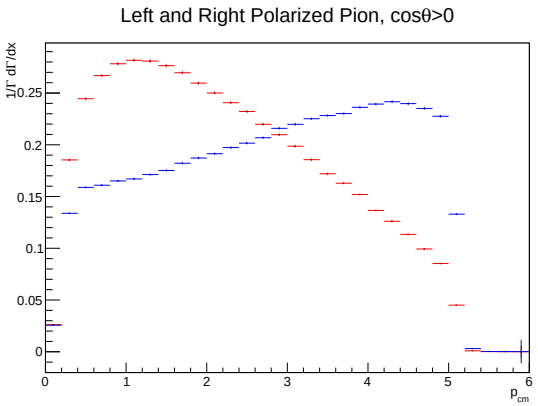

(c) $\tau \to \pi\nu$ momentum of final state particle

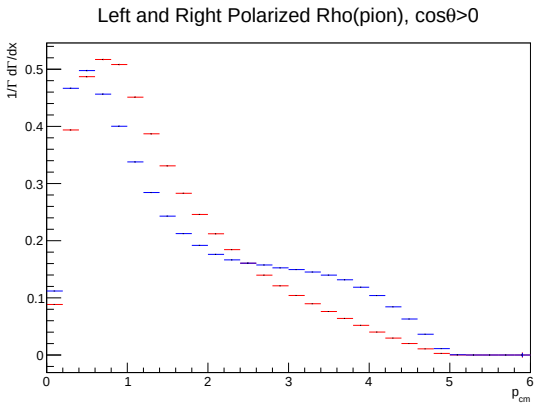

(d) $\tau \to \rho\nu$ momentum of final state particle

Figure 2: The sensitivity to the beam polarization for the different tau decay modes is shown above. The blue points are for a left handed electron beam, while the red points correspond to the right handed beam. In all plots only the forward region of the detector is shown for simplicity, however it should be noted the polarization sensitivity in the momentum is reversed in the backward region. Figure 2c shows the largest amount of polarization sensitivity and thus motivates the use of this decay mode in this study. In the case of the Rho decay (Figure 2d) there is some significant polarization sensitivity present and momentum is not the most optimal observable to see this difference. This decay mode will likely be studied in the future.

6.1 Event Selection

In order to select events with $\tau \to \pi\nu$ decays a few different event topologies were investigated for feasibility as summarized in table 3. It was found that for the 1v1 modes with 2 pions or a lepton and a pion that the $\tau^+\tau^- \to \ell^+\ell^-\bar{\nu}_\ell\nu_\tau$ modes swamped the polarization sensitivity remaining in the pions. In the case of a 3v1 topology

there was a small amount of backgrounds from $c\bar{c}$ processes but the mode would likely have sensitivity. Requiring one tau decays through a rho while the other is a pion turned out to have negligible amounts of non-tau backgrounds as well as the high branching fraction for $\tau \to \rho\nu_\tau$ produces the highest statistics of these potential modes.

With ρ tag chosen as the topology to be studied the following cuts were applied to the data to achieve a highly pure τ sample

1. Events pass the BaBar Tau Background Filter
2. Total charge of the event is zero
3. 2 charged tracks
4. Tracks are separated by $> 90^\circ$
5. The event P_T is > 1.2 GeV
6. One charged track looks like a rho
   - Option 1: One neutral cluster with a high pi0 PID likelihood
   - Option 2: Two neutral clusters with an invariant mass between 115 and 150 MeV
7. The rho hemisphere is free from other neutral clusters
8. The signal track has a hemisphere free from neutral clusters
9. The signal track fails an electron and muon PID selector

6.2 Polarization Fit

The beam polarization of a data set is extracted through a Barlow template fit. The event selection criteria is applied to Tau Monte-Carlo with each beam polarization state to produce a template for the kinematics of left or right polarized electron beams. The MC is split based on the signal track charge and placed into two dimensional histograms, binned by momentum and $\cos\theta$. The Barlow fit is fed the left and right polarized tau templates as well as templates for the non-tau MC modes. The non-tau MC modes (bhabhas,mumu,uds, and ccbar), are scaled by luminosity and fixed in the fit. The left and right components are allowed to freely vary their contribution to the fit between 0 and 1, with the expected result being roughly 0.5 and 0.5 for an unpolarized sample.

When the fit is preformed on either the unpolarized Tau MC or the data there are five pieces of information extracted. The contribution from the left and right polarized templates (L and R), the errors on those numbers (σ_L and σ_R), and the covariance of the left and right components (ρ). The polarization is then measured as shown in Equation 3 and the error as shown in Equation 4. The final measurement for a sample of data or MC is then found from the weighted average of the positive and negative charge.

$$P = L - R \tag{3}$$

$$\sigma_P^2 = \sigma_L^2 + \sigma_R^2 - 2\rho\sigma_L\sigma_R \tag{4}$$

Figure 3 shows an example of the polarized templates and unpolarized Tau MC used in the fit.

Decay Mode	Branching Fraction (%)
$\tau^- \to e^-\bar{\nu_e}\nu_\tau$	17.82±0.04
$\tau^- \to \mu^-\bar{\nu_\mu}\nu_\tau$	17.39±0.04
$\tau^- \to \pi^-\nu_\tau$	10.82±0.05
$\tau^- \to \pi^-\pi^0\nu_\tau$	25.49±0.09

Table 2: Tau decay branching fractions[**?**]

Mode	Event Topology	Comment
$\pi^+\pi^-$	$\tau^+\tau^- \to \pi^+\bar{\nu_\tau} + \pi^-\nu_\tau$	large contamination from $e^+e^- \to \mu^+\mu^-$
e tag	$\tau^+\tau^- \to e^+\bar{\nu_\tau}\nu_e + \pi^-\nu_\tau$	large contamination from $e^+e^- \to e^+e^-$
3vs1	$\tau^+\tau^- \to a_1^+\bar{\nu_\tau}(a_1^+ \to \pi^+\pi^+\pi^-) + \pi^-\nu_\tau$	low statistics and notable $c\bar{c}$ backgrounds
ρ tag	$\tau^+\tau^- \to \rho^+\bar{\nu_\tau}(\rho^+ \to \pi^+\pi^0) + \pi^-\nu_\tau$	negligible backgrounds and high statistics

Table 3: Tau Pair Decay Topologies

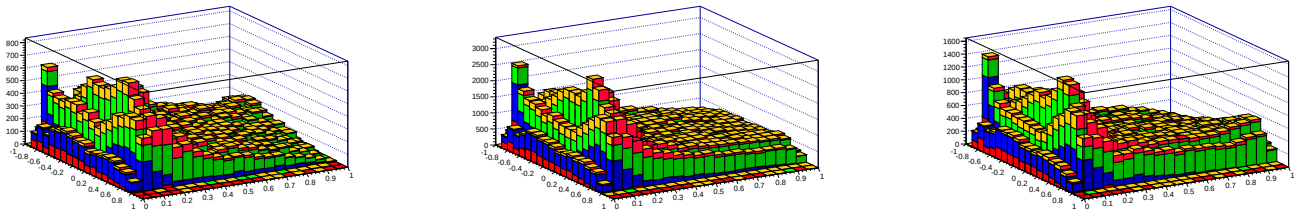

Figure 3: Left:Left polarized, Center:Unpolarized, Right:Right polarized; Distribution of $\cos\theta$ and momentum for the Tau MC templates and measured sample. Red is electrons, Blue is muons, Green is pions, Orange is other Tau decays

7 Schedule

8 Work Packages

9 Cost Estimates

10 Summary and Conclusions

References

[1] T. Abe *et al.* Belle II Technical Design Report, KEK Report 2010-1, Edited by Z. Dolezal and S. Uno, arXiv:1011.0352 (2010).

[2] ALEPH and DELPHI and L3 and OPAL and SLD Collaborations and LEP Electroweak Working Group and SLD Electroweak Group and SLD Heavy Flavour Group (S. Schael et al.), " Precision electroweak measurements on the Z^0 resonance", Phys.Rept. 427 (2006) 257-454.

[3] M. Baszczyk *et al.* (SuperB Collaboration), "SuperB Technical Design Report", INFN-13-01/PI, LAL 13-01, SLAC-R-1003, arXiv:1306.5655 [physics.ins-det].

[4] A. Aleksejevs, S. Barkanova, C. Miller, J.M. Roney and V. Zykunov, "NLO Radiative Corrections for Forward-Backward and Left-Right Asymmetries at a B-Factory", arXiv:1801.08510.

[5] J. Erler and A. Freitas "ElectroweakModel and Constraints on New Physics" in M. Tanabashi *et al.* (Particle Data Group), Phys. Rev. D**98**, 030001 (2018); J. Benesch *et al.* (Moller Collaboration), "The MOLLER Experiment: An Ultra-Precise Measurement of the Weak Mixing Angle Using Møller Scattering", JLAB-PHY-14-1986, arXiv:1411.4088v2 [nucl-ex] 2014; D. Becker *et al.* "The P2 experiment", arXiv:1802.04759 [nucl-ex] 2018.

[6] Uli Wienands, private communication

[7] M. Pospelov and A. Ritz, "Astrophysical Signatures of Secluded Dark Matter", Phys. Lett. B671:391397, 2009.

[8] N. Arkani-Hamed, D. P. Finkbeiner, T. R. Slatyer, and N. Weiner, "A Theory of Dark Matter", Phys. Rev. D79:015014, 2009.

[9] B. Batell, D. McKeen, and M. Pospelov, "New Parity-Violating Muonic Forces and the Proton Charge Radius", Phys.Rev.Lett. 107:011803, 2011. arXiv:1103.0721 [hep-ph].

[10] R. Pohl, A. Antognini, F. Nez, F. D. Amaro, F. Biraben, et al., "The size of the proton", Nature 466:213216, 2010.

[11] H. Davoudiasl, H. S. Lee and W. J. Marciano, Phys.Rev. D 92, no. 5, 055005 (2015)